A Hybrid Method for the Cross Flow Compact Heat Exchangers Design

G. Starace*, M. Fiorentino, M. P. Longo, E. Carluccio
Department of Engineering for Innovation, University of Salento,
via per Monteroni, Lecce 73100, Italy
*Corresponding author: giuseppe.starace@unisalento.it
tel.: +39 0832 297753 fax: +39 0832 297777

Abstract

Despite their limitations, the cross flow compact heat exchangers are generally modeled by the *ε-NTU* and LMTD methods and this mainly leads to the absence of effective consideration on the heat transfer geometry at the micro scale. At the same time, numerical analysis applied to compact cross flow heat exchangers, having different and complex finned surfaces respectively at the hot and cold sides, involves high computational costs.

A powerful alternative design procedure is here proposed that takes advantage of both numerical and analytical approaches. Hot and cold sides are numerically modeled and predictor functions for heat transfer and fluid dynamic performance are obtained with regression technique, for both sides.

The whole cross flow heat exchanger is divided into a set of control volumes, including the fins geometry 3D accurate description of both sides and their separation wall. An analytic iterative method is then used to find a wall temperature distribution throughout and to determine the mass flow rate distributions on both sides starting from the results of the numerical analysis at the micro scale.

The multi-scale approach leads to a better accuracy level with respect to the full-scale one and allows to profitably investigate different fins influence on flow distributions, local heat transfer and pressure losses through both sides of the heat exchanger.

Nomenclature

A	Heat transfer surface [m^2]
c_p	Specific heat at constant pressure [$J \cdot kg^{-1}K^{-1}$]
e	Percentage deviation
f	Response variable
i, j	Indexes
k	Total number of explanatory variables
$\dot{m}$	Mass flow rate [$kg \cdot s^{-1}$]
n	Samples number
p	Pressure [Pa]
Q	Heat transfer rate [W]
R^2	Coefficient of determination
SS_{res}	Sum of squares of residuals
SS_{tot}	Total sum of squares
T	Temperature [K]
U	Overall heat transfer coefficient [$W \cdot m^{-2}K^{-1}$]

v	Velocity [m/s]
V	Volumetric flow rate [m^3s^{-1}]
x, y, z	Spatial coordinates

Greek symbols

$(\beta_0\ \beta_1\ \beta_2\ \beta_3\ \beta_4\ \beta_5\ \beta_6\ \beta_7\ \beta_8\ \beta_9)$	Regression coefficients
ε	Effectiveness [-]
ρ	Density [$kg \cdot m^{-3}$]

Abbreviations

CS, HS	Cold side, Hot side
TSU	Surface Transfer Unit
$UHTV$	Unitary Heat Transfer Volume
$NTU, LMTD$	Number of Transfer Units, Log Mean Temperature Difference

Subscripts and Superscripts

adj	Adjusted
c, h	Cold fluid, Hot fluid
in, out	Inlet, Outlet
max	Maximum
T	Transposed
w	Wall

Introduction

The cross flow compact heat exchangers are widely used in civil and industrial applications where limited dimensions are required, thanks to their high surface area to volume ratio.

The cross flow compact heat exchangers are generally modeled by the *ε-NTU* [1] and LMTD methods despite their limitations that mainly consist of the absence of any influence in the calculations on the heat exchanger geometry at the micro scale. Therefore, their application to the design process compels engineers to oversize dimensions in order to ensure the performance requirements.

A detailed review of solution methods for simple and complex heat exchangers was made by Sekulić et al [2]. The *ε - NTU* functions were obtained either with analytical, or approximate or numerical methods, or matrix formalism or additional methods based on the heat exchanger configurations.

Navarro et al [3] developed a numerical methodology to obtain *ε – NTU* data for standard and complex configurations. They divided the heat exchanger into a set of control volumes identified as one-pass mixed or unmixed cross-flow heat exchanger and applied the governing equations to each element. The system of equations for the whole heat exchanger was then solved iteratively.

Sanders et al [4] studied a particular compact heat exchanger with louvered fins equipped with special winglets. The winglets placed on the louvers showed an improvement in the heat transfer rate along the tube wall, but the geometry complexity did not allow the use of classical methods. They carried out experimental analyses as well on the louvered fin heat exchanger, reaching an optimal configuration for the geometrical characteristics of the fin.

Lawson at al [5] continued the work of Sanders [4] focusing on the effect of winglets and piercings on tube wall.

The numerical analysis of heat exchanger through CFD methods (for design and optimization) has greatly taken advantage from high performance processors.

In Bhutta et al. [6] an excursus on the application of CFD in the field of heat exchanger was carried out; CFD was found to be employed to investigate several and different aspects such as fluid flow maldistribution, fouling, pressure drop and thermal analysis.

Ferouillat et al. [7] studied the vortex generator technology, that provided both heat transfer and mixing, through a pair of delta winglets and a pair of rectangular winglets. The authors successfully evaluated the performance of that device using the CFD.

Stalio et al. [8] modeled the heat and mass transfer in sinusoidal symmetric wavy channels with an iterative numerical algorithm.

Despite the efforts of many authors, the CFD analysis of different combination of fins at both sides (hot and cold fluid) of the heat exchanger involves high computational costs, and, as a consequence, an alternative procedure could be highly appreciated by researchers and designers.

Scattina et al [9] suggested a methodology based on CFD simulations of small portions of the cross flow compact heat exchanger. The results were up-scaled to the whole system by the *ε-NTU* method.

Here an innovative method called “hybrid method” aimed to obtain the overall heat exchanger performance starting from the CFD simulation data at the micro-scale is proposed.

The whole heat transfer surface is divided into a set of control volumes that include the fins of both the cold and hot side. These volumes are then processed by a routine that couples the performance by both sides starting from given operating conditions in terms of flow rates and inlet temperatures.

The results of the separate numerical modeling of the two finned surfaces carried out by Carluccio et al. [10] and [11] are here used to show how to get prediction functions for heat transfer performance as well as pressure losses and temperature fields through a purposely defined regression technique for a case study. The predictor functions allow to accurately extend the numerical results relevant to a sub-domain to the whole heat exchanger drastically reducing the computational cost for a given configuration.

The cross flow heat exchanger geometrical description to be considered for the method application

The compact cross flow heat exchanger under examination can be considered in its construction basically as made up by successive layers.

Each layer (Fig.1) consists of the two sides. In the case study here taken into consideration, in order to better describe the new method, respectively offset strip fins at the HS and wavy at the CS are installed, as illustrated in Fig.2.

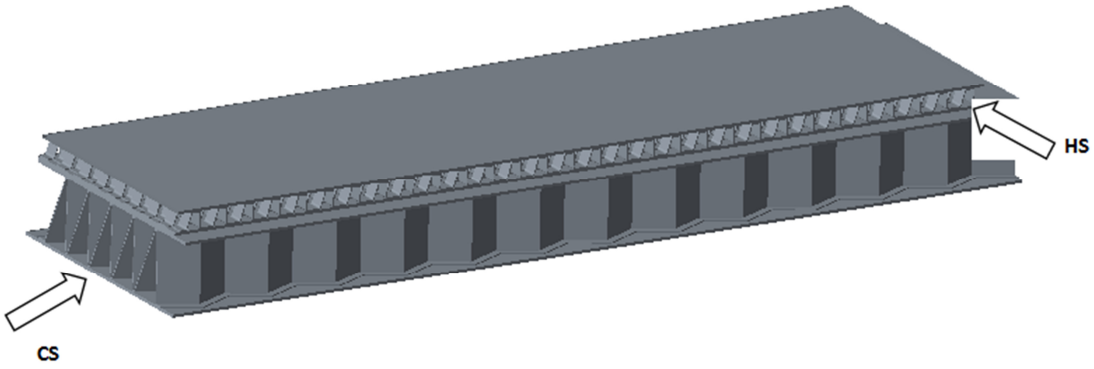

Figure 1. A single layer that will be made up in the stack together with the others.

The performance of the whole heat exchanger is obtained assuming a uniform distribution of the fluid along the stack and multiplying the heat transfer rate corresponding to the single layer by the layers number provided for the stack.

A control volume (TSU) was detected for each side containing half of the wall thickness that divides the two sides, as illustrated in Fig.3.

The CFD analyses of the TSUs that have been considered for the case study were carried out during previous works by Carluccio et al. in [10] and [11], whose results were in good agreement with data available from literature. They were completed with the same approach, until reaching a suitable number of runs with defined operating conditions, in order to meet the requirements of the application of the hybrid method here presented.

For both cold and hot fluids simulations, mass flux through the faces separating adjacent cells was set to zero as this was considered a sufficient approximation to the aim of the method.

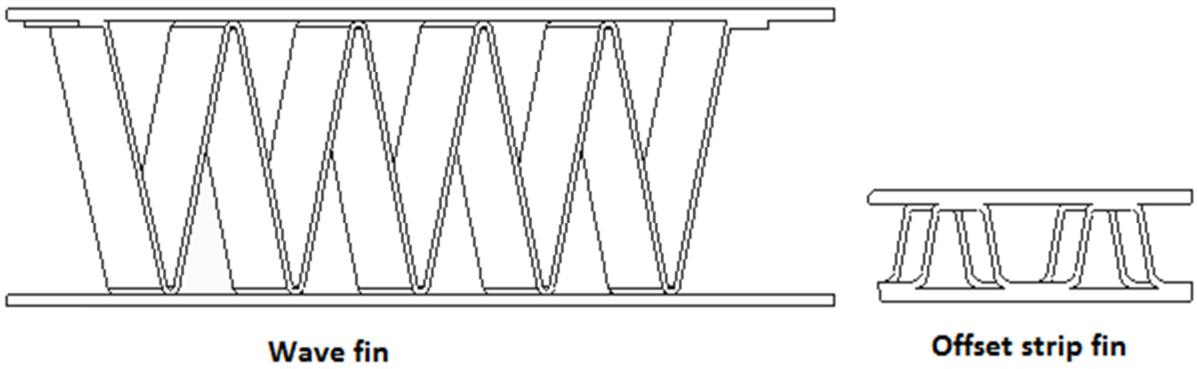

Figure 2. Fins used in the case study, whose first results and description are available in Carluccio et al. [10] and [11].

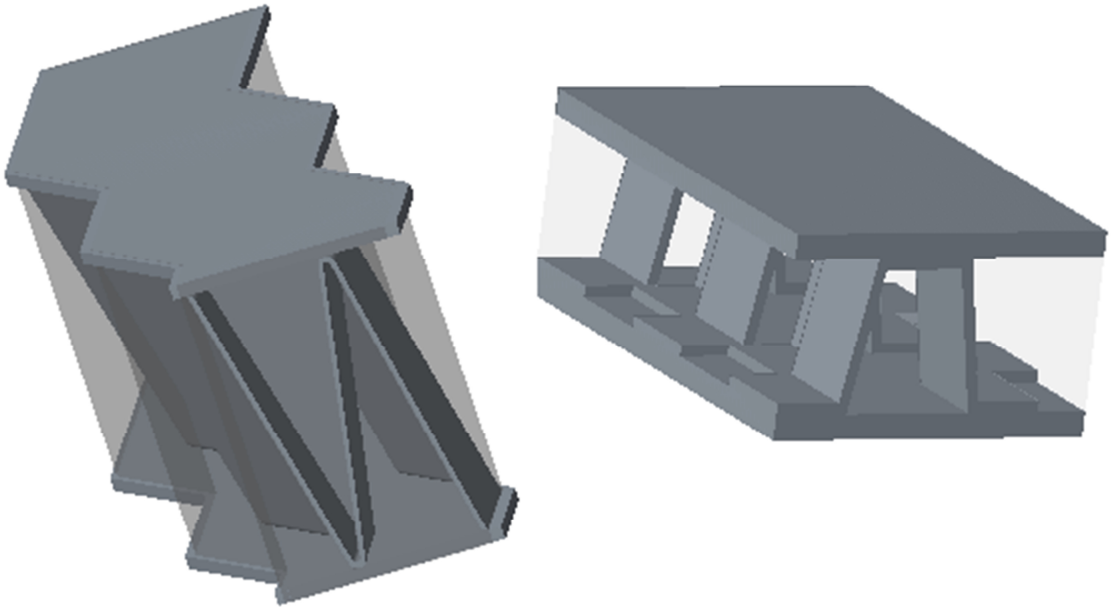

Figure 3. TSU for CS and HS.

The UHTV was defined as the volume containing both the TSUs, whose rectangular section that operates as the separation wall can be observed in Fig.4.

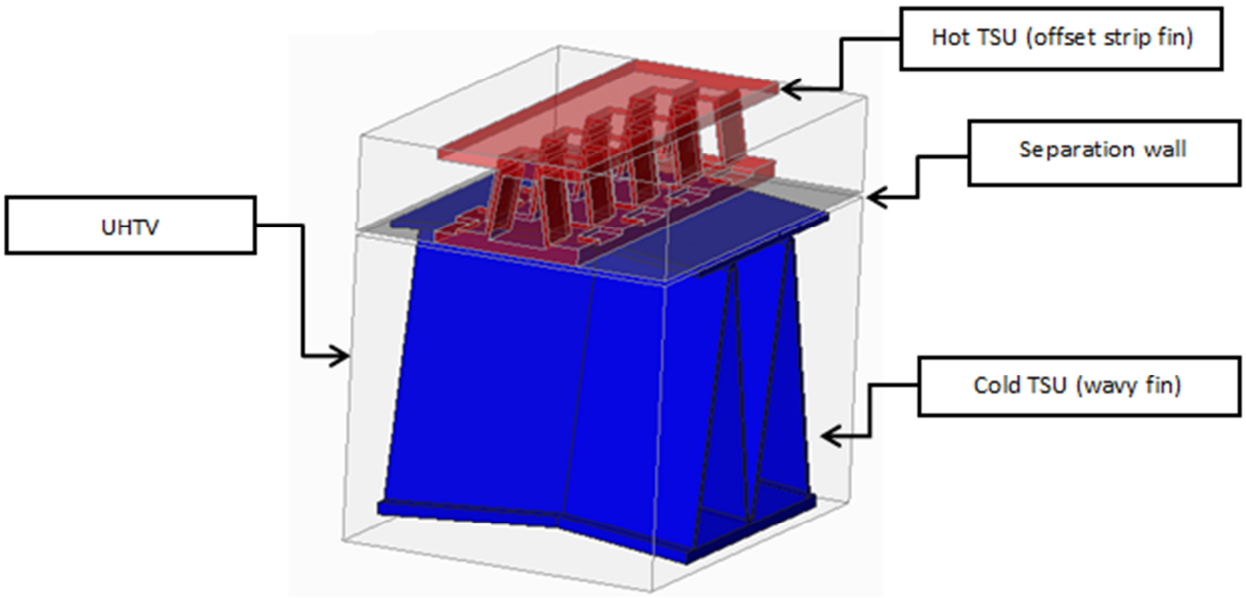

Figure 4. UHTV scheme. Here the particular case taken into consideration for the hybrid method description.

Each layer is schematized as a matrix whose single elements (i, j) are associated at each UHTV.

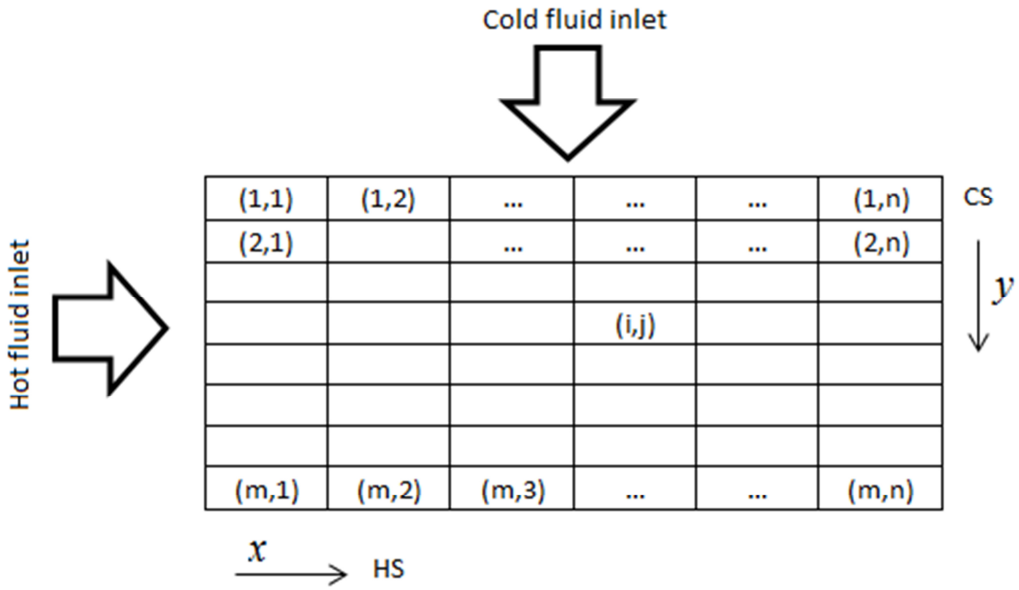

Figure 5. UHTVs coordinates schematization in the layer.

Mathematical model

Referring to a single TSU, the explanatory variables (CFD inputs), for both hot and cold sides, are:

- the temperature at the inlet T_{in};
- the velocity at the inlet v_{in};
- the wall temperature T_w;

while the response variables (CFD outputs) are

- the temperature at the outlet T_{out};
- the velocity at the outlet v_{out};
- the pressure drop Δp.

The results of numerical simulations represent the control points to perform the regression. Each response variable is expressed as

$$f = (\beta_0\ \beta_1\ \beta_2\ \beta_3\ \beta_4\ \beta_5\ \beta_6\ \beta_7\ \beta_8\ \beta_9)(1\ \ V_{in}\ \ T_{in}\ \ T_w\ \ V_{in}T_{in}\ V_{in}T_w\ \ T_{in}T_w\ V_{in}^2\ \ T_{in}^2\ \ T_w^2)^T \quad (1)$$

The chosen regression model is quadratic and includes constant, linear, interaction and squared terms.

The regression coefficients $(\beta_0\ \beta_1\ \beta_2\ \beta_3\ \beta_4\ \beta_5\ \beta_6\ \beta_7\ \beta_8\ \beta_9)$ are different for each response variable.

The algorithm works as follows:

$\underline{Cell\ (1,1)}$

Considering the matrix element $(i,j)$with *i* and *j* indexes equal to 1, the inlet temperature is known, for both cold and hot sides.

The inlet velocity is obtained by assuming a uniform distribution of the mass flow rate in the cells of the first row (for the cold side) and of the first column (for the hot side).

The wall temperature is firstly assumed equal to the mean value between the cold and hot fluid temperatures at the inlet:

$$T_w(1,1) = \frac{T_{in,c}(1,1) + T_{in,f}(1,1)}{2} \quad (2)$$

V_{out}, T_{out}, Δp are then determined through Eq. [1].

The heat transfer rate at the UHTV scale is determined as

$$Q_h(1,1) = \dot{m}_h(1,1)c_{p,h}(T_{in,h}(1,1) - T_{out,h}(1,1)) \quad (3)$$

$$Q_c(1,1) = \dot{m}_c(1,1)c_{p,c}(T_{out,c}(1,1) - T_{in,c}(1,1)) \quad (4)$$

The heat transfer rates at the hot and cold sides are compared: the difference represents the convergence condition and affects the iteration number. A new value of wall temperature has to be assumed until the convergence condition is not yet reached.

$\underline{Cell\ (i,j)}$

Considering the generic $Cell\ (i,j)$, the temperature and velocity at the inlet for the hot side are

$$T_{h,in}(i,j) = T_{h,out}(i,j-1) \tag{5}$$

$$v_{h,in}(i,j) = v_{h,out}(i,j-1) \tag{6}$$

1 while for the cold side

$$T_{c,in}(i,j) = T_{c,out}(i-1,j) \tag{7}$$

$$v_{c,in}(i,j) = v_{c,out}(i-1,j) \tag{8}$$

2 Assuming a tentative value of the wall temperature, the same calculation scheme of $Cell\,(1,1)$ is
3 applied to each $Cell\,(i,j)$.
4 The response variables are so obtained for any element of the matrix.
5 A check on the pressure load is then performed.
6 The pressure load at the cold side, corresponding to the j -th column is determined as

$$\Delta p_{c,j} = \sum_{i=1}^{m} \Delta p_c(i,j) \tag{9}$$

7 The condition of a pressure constant for any column is then considered

$$\Delta p_{c,1} = \Delta p_{c,2} = \cdots = \Delta p_{c,j} = \cdots = \Delta p_{c,n} \tag{10}$$

8 The same condition is imposed for the hot fluid:

$$\Delta p_{h,i} = \sum_{j=1}^{n} \Delta p_h(i,j) \tag{11}$$

$$\Delta p_{h,1} = \Delta p_{h,2} = \cdots = \Delta p_{h,i} = \cdots = \Delta p_{h,m} \tag{12}$$

9 If conditions (10) and (12) are not satisfied, a new distribution of the mass flow rate is assumed, by
10 varying the mass flow rate in any UHTV of a quantity proportional to the pressure drop deviation
11 from the mean value. The mass flow rate in the last UHTV is calculated as difference between the
12 total mass flow rate and the sum of mass flow rates in the previous ones. This accounts for the mass
13 conservation condition for both sides.
14 Steps 1-12 are repeated until the check on the pressure drop is not satisfied.
15 The flow diagram of the algorithm implemented in Matlab is shown in Fig.6.

16 **Regression technique**

CFD analyses have been carried out by considering air (at ambient pressure) as fluid at both hot and cold sides. The thermo-physical properties of the fluids in the heat exchanger considered for the case study are listed in Tab.1.

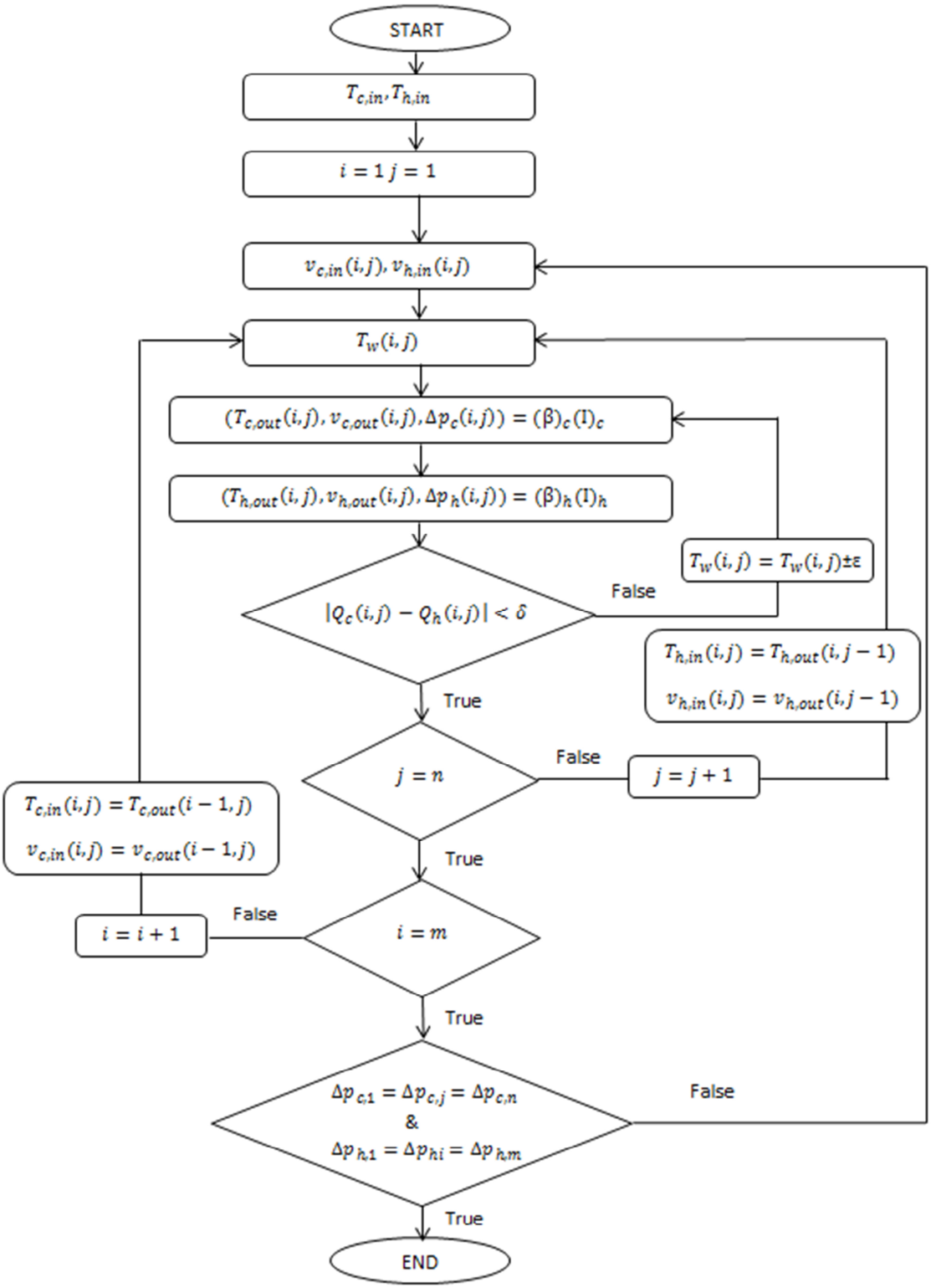

Figure 6. Algorithm flow diagram of the hybrid method.

The numerical simulations inputs and results [10] and [11] for both the hot and cold sides are listed in Tab.2 and 3 respectively.

Table 1. Thermophysical properties of hot and cold fluids considered in the case study.

	Unit	Air at HS	Air at CS
c_p	J/(kg·K)	1006.43	1006.43
ρ	kg/m^3	Ideal gas	1.225

Table 2. Input and output values of CDF simulations for HS for the case study.

Explanatory variables			Response variables		
$v_{h,in}$ [m/s]	$T_{h,in}$ [K]	T_w [K]	Δp_h [Pa]	$v_{h,out}$ [m/s]	$T_{h,out}$ [K]
18	433	345	142.85	18.16	409.39
18	433	365	147.73	18.42	414.79
18	433	325	137.72	17.88	403.56
44	433	365	736.96	44.30	419.90
11	433	365	64.52	11.52	411.23
44	433	325	697.74	43.41	412.02
11	433	325	59.76	11.16	397.72
18	380	345	170.41	18.67	371.24
44	380	345	852.00	44.43	373.60
11	380	345	74.02	11.71	369.55
18	380	365	176.68	18.95	376.45
44	380	365	877.40	45.34	377.29
18	380	325	164.13	18.38	365.99
44	380	325	827.02	44.40	369.91
11	380	325	71.10	11.50	363.22
44	330	325	997.00	45.48	329.01
44	433	345	498.64	43.82	417.03
11	433	345	62.21	11.32	404.68
11	433	433	72.30	11.12	433.00
18	433	433	164.42	19.29	433.00
44	433	433	807.29	45.77	433.00
11	380	380	78.85	10.71	380.00
18	380	380	180.00	17.42	380.00
44	380	380	896.75	45.68	380.00
11	330	330	86.72	11.94	330.00
18	330	330	200.97	17.39	330.00
44	330	330	1007.40	45.61	330.00
11	303	303	91.88	11.87	303.00
18	303	303	214.48	17.78	303.00
44	303	303	1081.80	45.58	303.00

Table 3. Input and output values of CFD simulations for CS for the case study.

Explanatory variables				Response variables	
$v_{c,in}$ [m/s]	$T_{c,in}$ [K]	T_w [K]	Δp_c [Pa]	$v_{c,out}$ [m/s]	$T_{c,out}$ [K]
18	303	345	497.39	19.12	324.62
36	303	365	1710.00	39.41	327.16
9	303	365	147.00	10.08	341.72
18	303	365	497.00	20.04	334.47
18	303	325	496.00	20.04	314.02
36	303	325	1704.00	39.41	311.64
9	303	325	144.78	9.97	316.64
36	303	345	1742.00	36.90	319.47
9	303	345	147.00	10.08	329.59
9	303	303	245.00	10.06	303.00
18	303	303	769.00	20.01	303.00
36	303	303	2426.00	39.32	303.00
4	303	345	62.25	4.30	333.97
4	303	365	62.25	4.30	348.85
4	303	325	62.24	4.30	319.09
4	303	303	62.27	4.30	303.00
0	303	303	0.00	0.00	303.00
18	346	365	771.00	20.03	355.47
4	325	345	66.36	4.29	339.73
9	310	325	240.23	9.96	319.19
4	273	325	62.21	4.29	311.39
4	273	345	62.21	4.29	326.27
4	273	365	62.21	4.29	341.14
4	323	345	62.19	4.29	339.02
4	323	365	62.24	4.29	353.89
18	273	325	759.47	19.27	300.14
18	273	345	760.09	19.27	310.67
18	273	365	755.01	19.27	323.85
18	323	345	759.38	19.27	334.29
18	323	365	759.17	18.79	344.24
36	273	325	2447.80	38.48	293.92
36	273	345	2450.71	38.48	302.05
36	323	325	2424.91	38.48	323.67
36	323	345	2433.35	38.48	331.68
36	323	365	2440.94	38.48	339.76
4	325	325	62.23	4.10	325.00
4	345	345	62.23	4.20	345.00
4	365	365	62.23	4.30	365.00
18	325	325	755.00	18.20	325.00
18	345	345	755.00	18.30	345.00
18	365	365	755.00	18.40	365.00
36	325	325	2426.00	36.40	325.00
36	345	345	2426.00	36.50	345.00
36	365	365	2426.00	36.70	365.00

Regression was performed with the following different orders to choose the most accurate with acceptable computational costs:

- First order (Linear);
- Second order with quadratic terms (Pure quadratic);
- Second order with interaction terms (Interaction);

- Second order with quadratic and interaction terms (Quadratic).

The accuracy of fit was evaluated through the adjusted coefficient of determination.
The coefficient of determination depends on the ratio between the sum of squares of residuals and the total sum of squares.

$$R^2 = 1 - \frac{SS_{res}}{SS_{tot}} \tag{13}$$

The adjusted coefficient was calculated as follows:

$$R^2_{adj} = R^2 - (1 - R^2)\frac{k}{n - k - 1} \tag{14}$$

A higher adjusted coefficient corresponds to a better approximation.
The adjusted coefficients of determination of the different regression models are summarized in Tab.4.

Table 4. . Adjusted coefficients of determination for HS for the case study.

	R^2_{adj}			
	First order	Second order with quadratic terms	Second order with interaction terms	Second order with quadratic and interaction terms
$v_{h,out}$	0.9983	0.9982	0.9990	0.9990
$T_{h,out}$	0.9964	0.9961	0.9996	0.9998
Δp_h	0.9502	0.9523	0.9816	0.9877

The regression of second order with quadratic and interaction terms (10 coefficients) was characterized by a higher adjusted coefficient of determination.
The quadratic model was able to predict values closer to the observed data and for this reason it was chosen for the present study.
The polynomial coefficients obtained with regression for hot and cold sides are shown in Tab.5 and 6.

Table 5. Regression coefficients for the HS for the case study.

	Δp_h	$T_{h,out}$	$v_{h,out}$
β_0	$3.8645 \cdot 10^{1}$	-2.3000	$1.3418 \cdot 10^{1}$
β_1	$2.9992 \cdot 10^{1}$	$2.8313 \cdot 10^{-1}$	$9.2150 \cdot 10^{-1}$
β_2	2.5022	$7.2415 \cdot 10^{-1}$	$5.7543 \cdot 10^{-4}$
β_3	-3.6397	$2.7285 \cdot 10^{-1}$	$-7.0755 \cdot 10^{-2}$
β_4	$-1.1117 \cdot 10^{-1}$	$3.7912 \cdot 10^{-3}$	$-6.3979 \cdot 10^{-4}$
β_5	$4.8316 \cdot 10^{-2}$	$-3.7537 \cdot 10^{-3}$	$7.3296 \cdot 10^{-4}$
β_6	$-4.3639 \cdot 10^{-3}$	$4.5083 \cdot 10^{-4}$	$2.9608 \cdot 10^{-4}$
β_7	$3.4693 \cdot 10^{-1}$	$-5.2771 \cdot 10^{-3}$	$1.4997 \cdot 10^{-3}$
β_8	$2.1003 \cdot 10^{-4}$	$-2.9856 \cdot 10^{-4}$	$-1.1761 \cdot 10^{-4}$
β_9	$6.6153 \cdot 10^{-3}$	$-1.4969 \cdot 10^{-4}$	$-8.3921 \cdot 10^{-5}$

Table 6. Regression coefficients for the CS for the case study.

	Δp_c	$T_{c,out}$	$v_{c,out}$
β_0	$7.1730 \cdot 10^{3}$	$-6.5571 \cdot 10^{1}$	$7.6794 \cdot 10^{1}$
β_1	$1.8035 \cdot 10^{1}$	$-3.9469 \cdot 10^{-1}$	$1.3482 \cdot$
β_2	$-3.6210 \cdot 10^{1}$	$4.4073 \cdot 10^{-1}$	$2.8823 \cdot 10^{-2}$
β_3	$-8.6873 \cdot$	$9.6341 \cdot 10^{-1}$	$-4.8703 \cdot 10^{-1}$
β_4	$4.2994 \cdot 10^{-2}$	$8.2553 \cdot 10^{-3}$	$-6.8531 \cdot 10^{-4}$
β_5	$-4.2596 \cdot 10^{-2}$	$-8.3099 \cdot 10^{-3}$	$-1.3527 \cdot 10^{-4}$
β_6	$-8.7207 \cdot 10^{-2}$	$-2.7958 \cdot 10^{-3}$	$5.8967 \cdot 10^{-4}$
β_7	$1.2910 \cdot$	$9.4067 \cdot 10^{-3}$	$-8.3639 \cdot 10^{-4}$
β_8	$1.0694 \cdot 10^{-1}$	$1.2848 \cdot 10^{-3}$	$-3.7509 \cdot 10^{-4}$
β_9	$5.0300 \cdot 10^{-2}$	$9.1821 \cdot 10^{-4}$	$4.6442 \cdot 10^{-4}$

Discussion and Results

The case study here presented consists of a single layer of a compact cross flow heat exchanger, being crossed by the mass flow rates at the inlet temperature at hot and cold sides summarized in Tab.7.

Table 7. Fluid properties at the inlet of the layer for the case study.

	Unit	Hot fluid	Cold fluid
$\dot{m}$	kg/s	$7.9 \cdot 10^{-3}$	$2.6 \cdot 10^{-2}$
T_{in}	K	433	303

The layer had dimensions 190 x 150 mm^2: the corresponding matrix had dimensions 3 x 15; this leads to a number of UHTVs of 45.

The cold fluid mass flow rate trend along the *x* direction (see Fig.5) is shown in Fig.7. It increases with *x*, getting the maximum value, $1.8 \cdot 10^{-3}$kg/s, at position *j*=10, and then it becomes asymptotic.

The maximum percentage deviation from the mean value of $1.75 \cdot 10^{-3}$kg/s, corresponding to a uniform distribution, occurs at position *j*=1 and is of 12.7%.

The mass flow rate of hot fluid can be considered constant with *y*; actually, the maximum percentage deviation from the mean value of $2.63 \cdot 10^{-3}$kg/s is equal to 0.87% at position *i*=1.

The local mass flow rates at the hot side are less dispersed with respect to the mean value, than those of the cold side, as the latter is distributed over a smaller number of cells.

The calculated mean pressure drops at cold and hot sides are summarized in Tab.8.

The maximum percentage deviations from the mean value are of 0.065 and 0.099% for hot and cold sides, respectively, as a consequence of a convergence criterion set to 0.1%.

The maximum deviations occur at *i*=1 for hot fluid and *j*=1 for cold fluid, where the mass flow rate

deviations from the mean value are the highest.

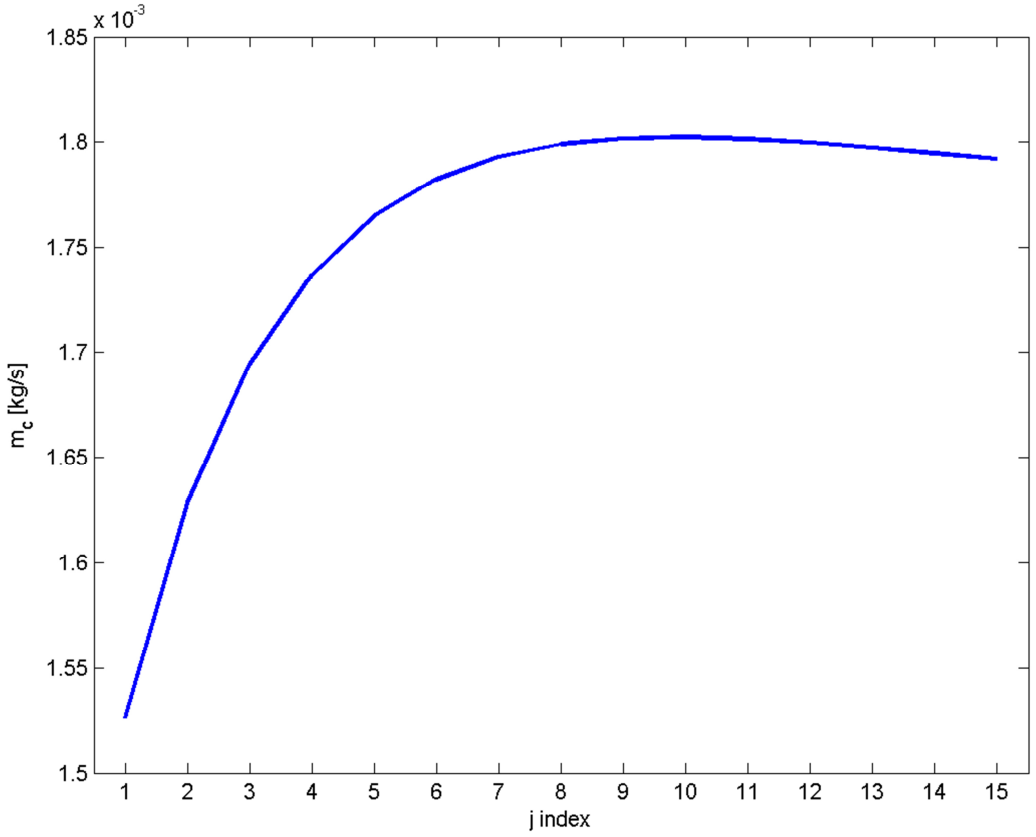

Figure 7. Cold fluid mass flow rate distribution at the HS for the case study.

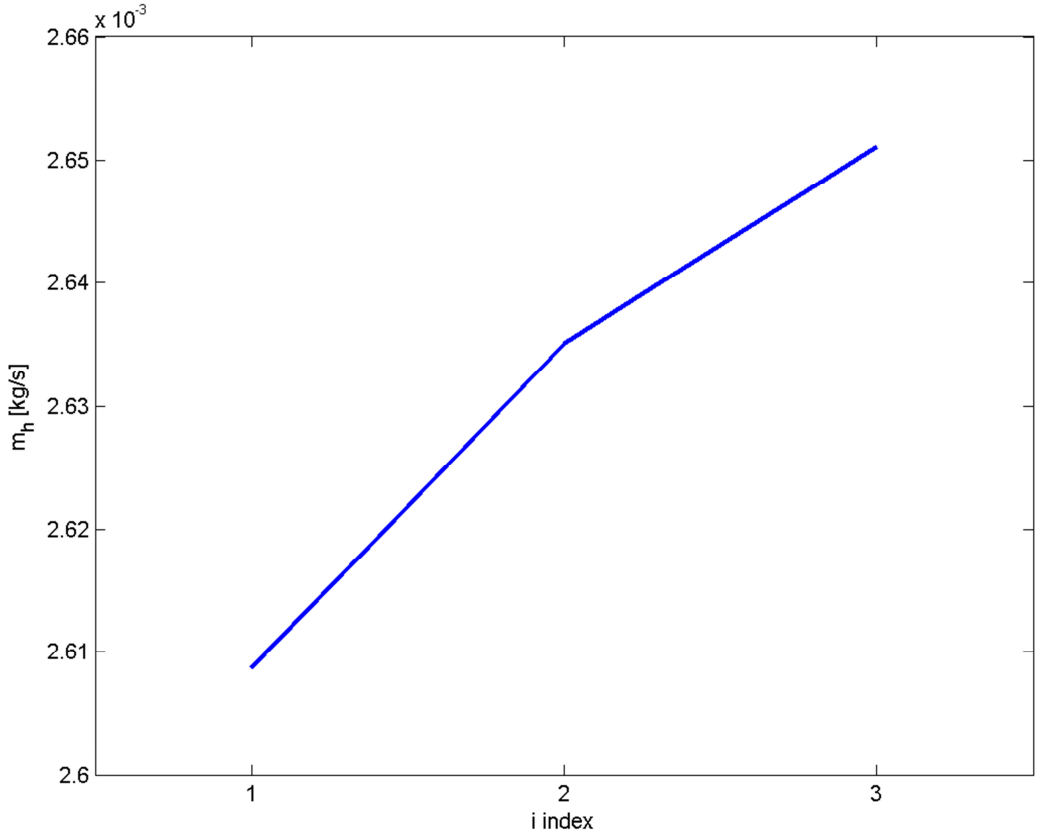

Figure 8. Hot fluid mass flow rate distribution at the CS for the case study.

Table 8. Pressure drops at hot and cold sides for the case study.

	Unit	Hot fluid	Cold fluid
Δp	Pa	4781	2372
e_{max}	%	0.065	0.099

The inlet temperature of cold fluid throughout the layer is illustrated in Fig.9. The temperature is uniform and equal to 303 K in all the UHTVs of the first row, corresponding to the fluid entrance, increases approaching the exit (along *y* direction) and the hot fluid inlet (on the left).

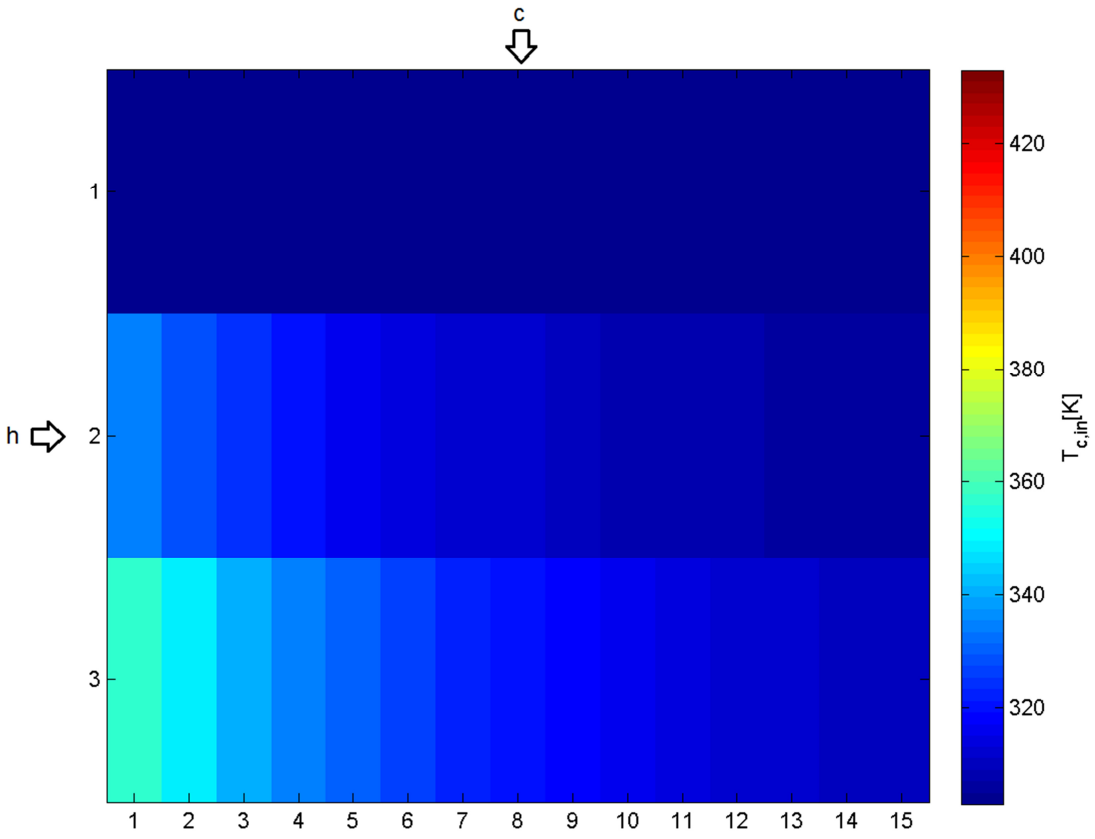

Figure 9. Cold fluid inlet temperature over the layer.

The hot fluid temperature can be seen (Fig.10) as equal to 433 K at the entrance (first column) and showing a decreasing trend along horizontal direction and near to the cold fluid inlet.

Fig. 11 shows wall temperature that decreases along the hot fluid direction and increases along the cold fluid direction.

The cold fluid temperature differences between inlet and outlet are shown in Fig.12.

The temperature difference decreases with *j* (along the hot fluid direction) and decreases with *i* for $j \leq 6$, while it increases with *i* for $j > 6$.

As can be observed in Fig.13, the same considerations are valid for the hot fluid temperature difference.

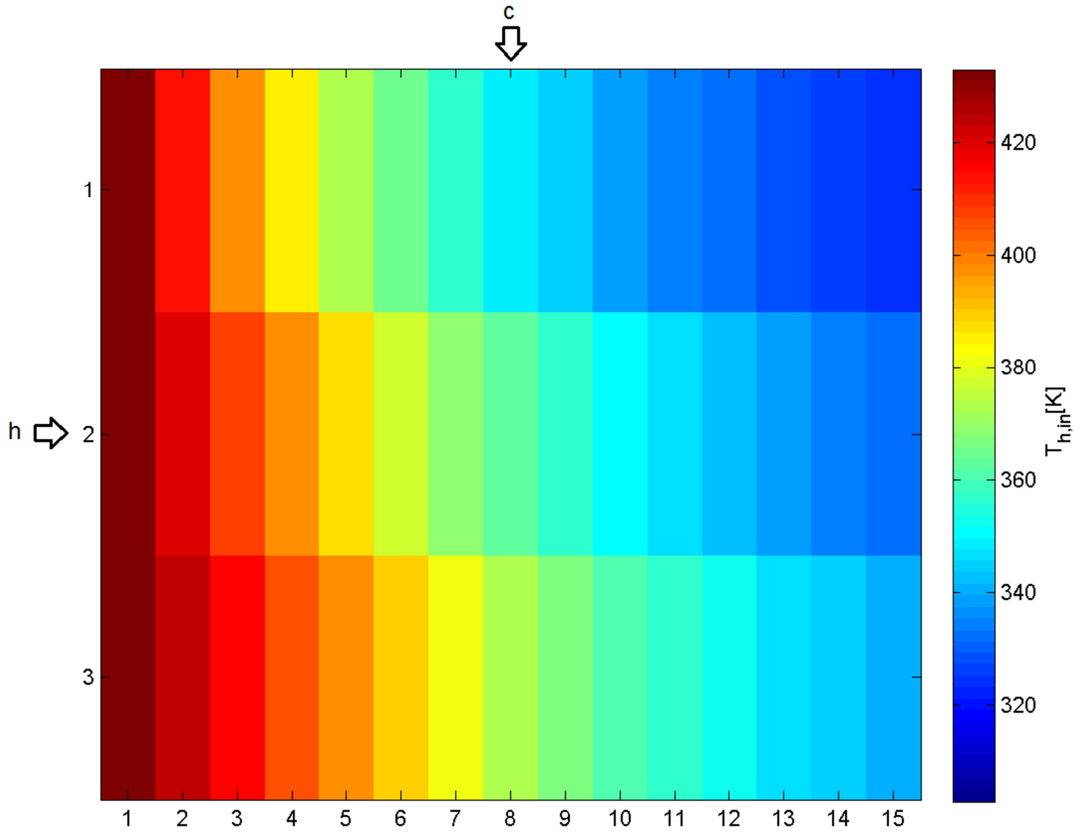

Figure 10. Hot fluid inlet temperature over the layer for the case study.

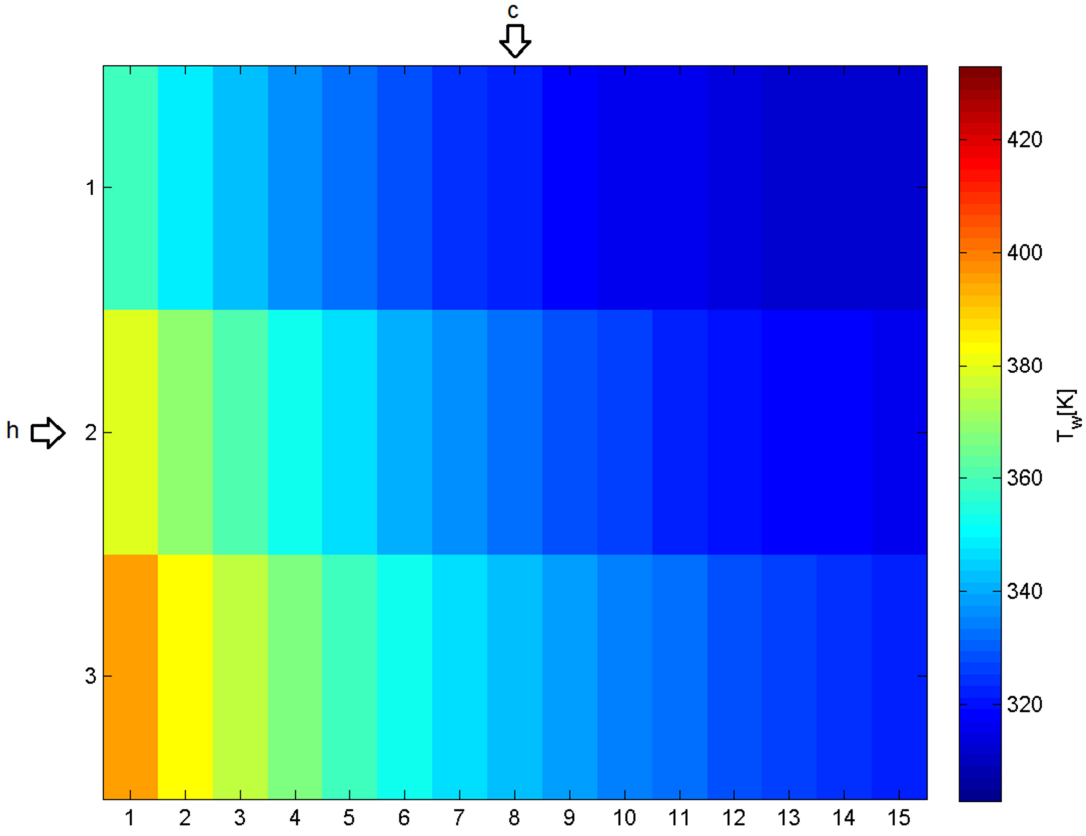

Figure 11. Wall temperature over the layer for the case study.

For this reason the maximum heat transfer rate occurs in the cell in the first row and column, while the minimum value corresponds to the cell in the first row and last column.

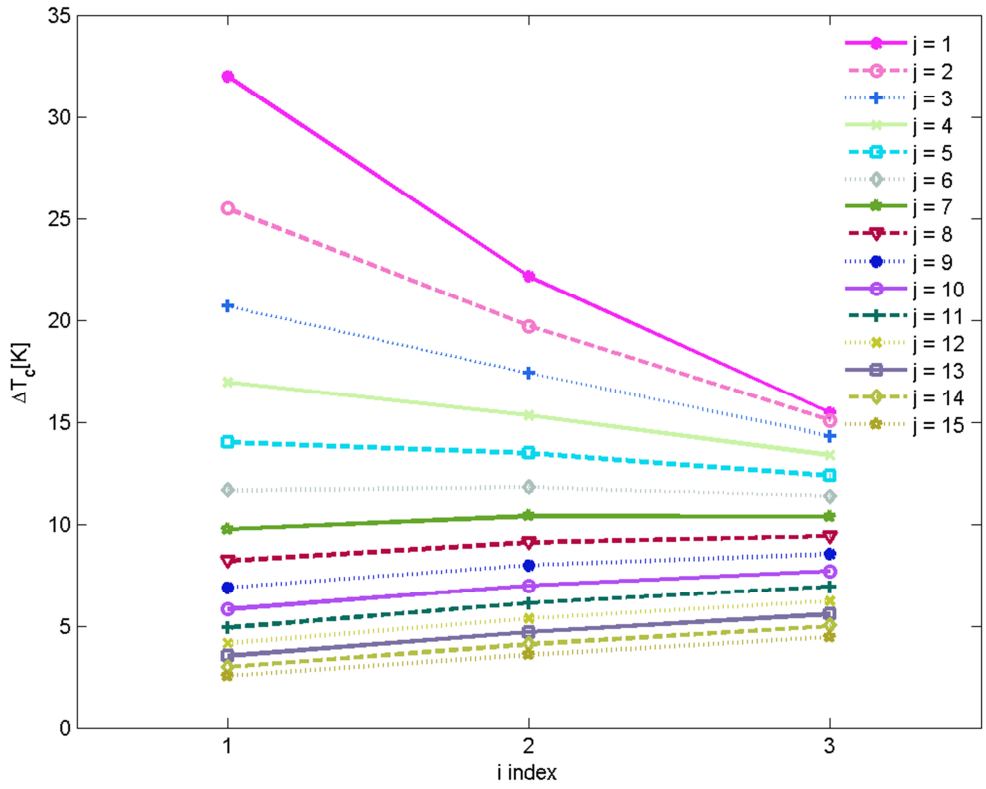

Figure 12. Cold fluid temperature difference between inlet and outlet along the CS for the case study.

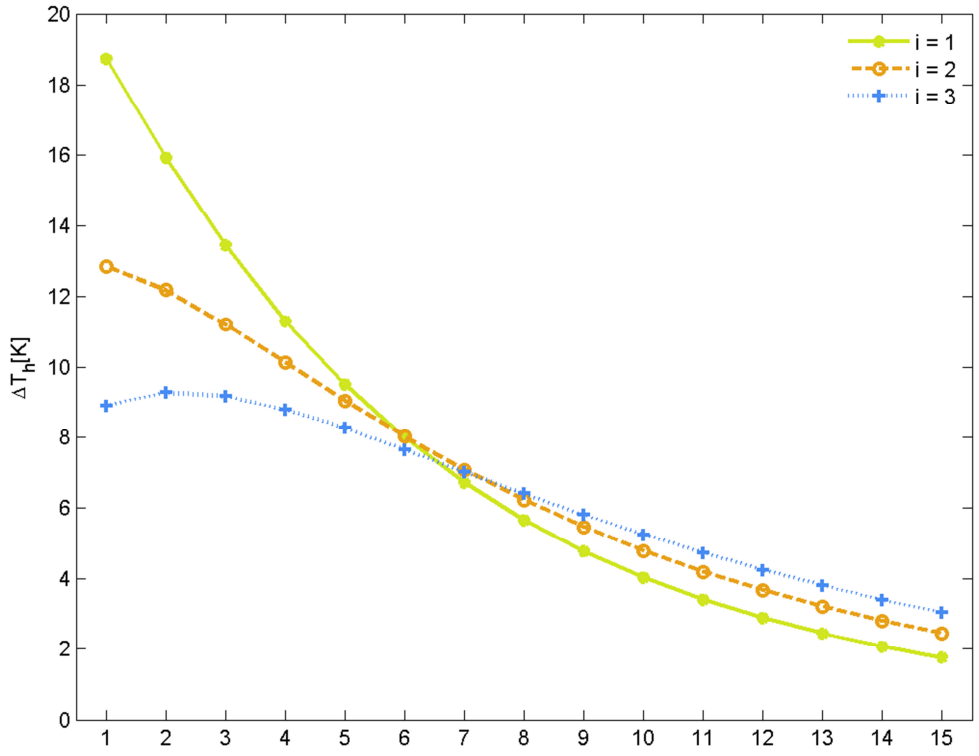

Figure 13. Hot fluid temperature difference between inlet and outlet along the HS for the case study.

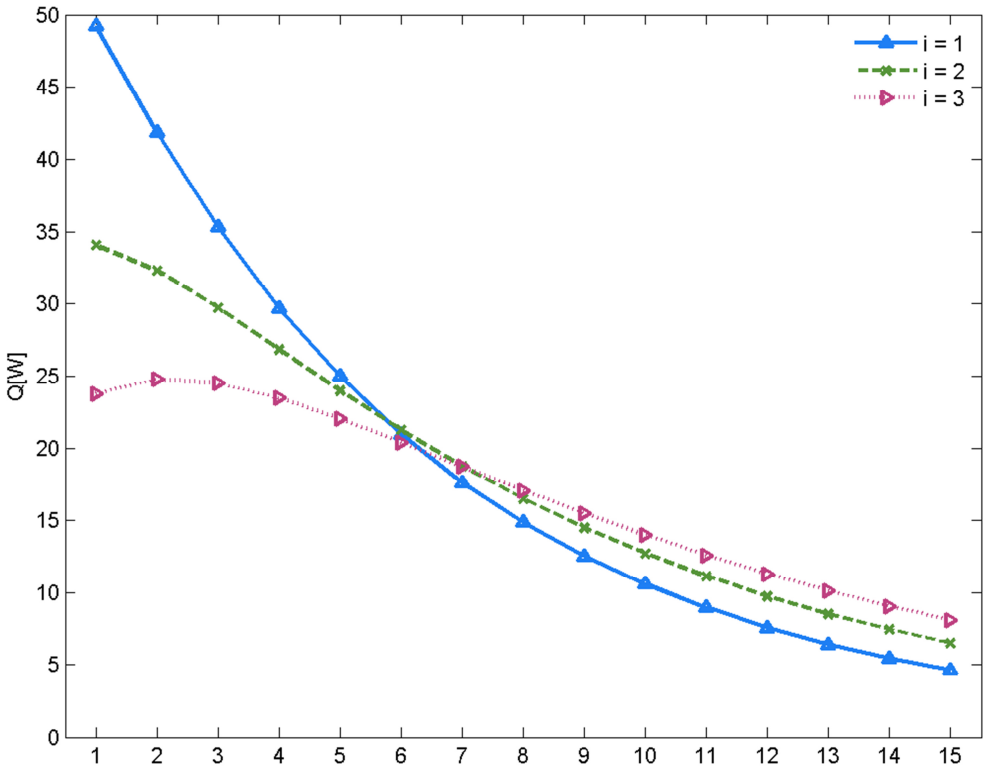

Figure 14. Heat transfer rate trend over the layer for the case study.

The maximum and minimum values of heat transfer rate are about 50 and 5 W, respectively. The convective heat transfer coefficients on the cold and hot sides, referred to the area of separation wall, are plotted in figures 15 and 16, respectively.

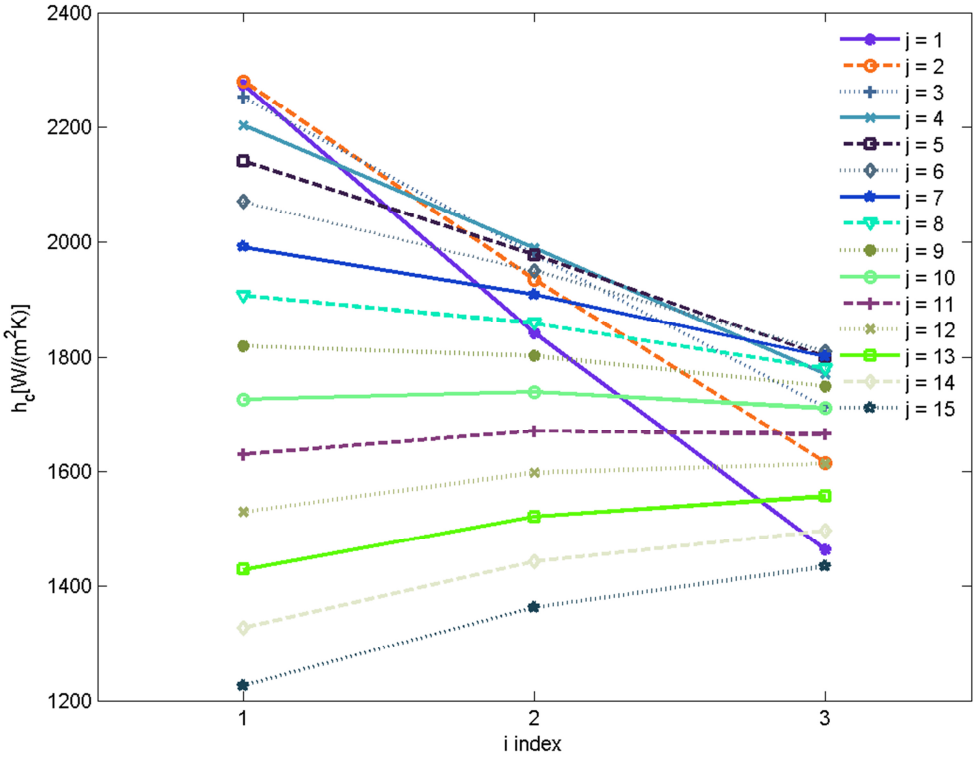

Figure 15. Convective heat transfer coefficient along the CS for the case study.

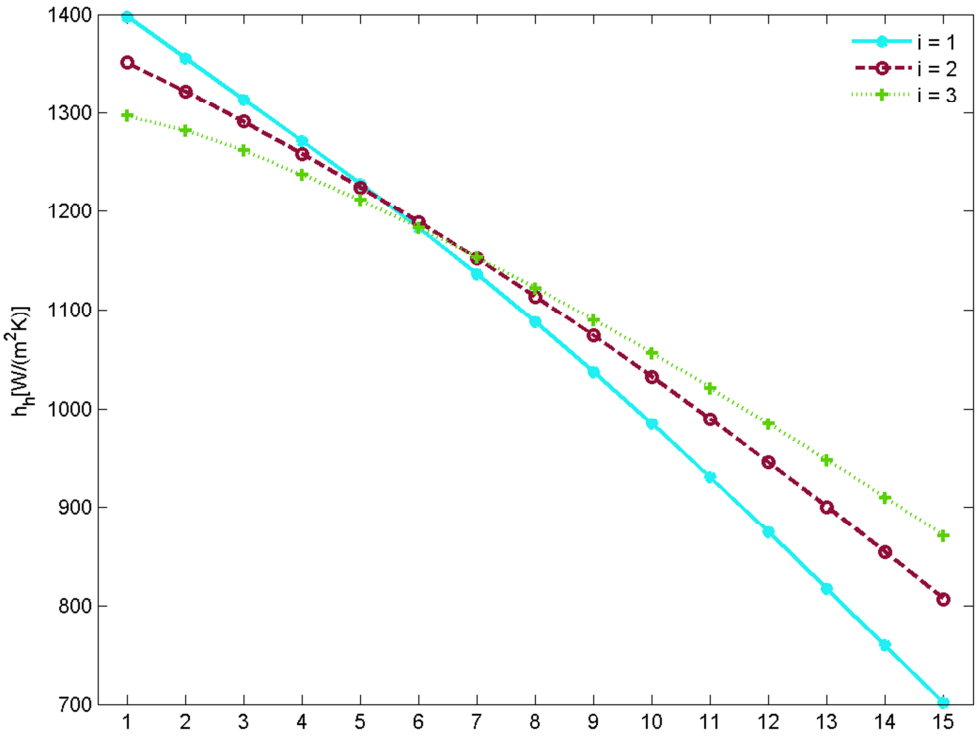

Figure 16. Convective heat transfer coefficient along the HS for the case study.

These figures suggest that the heat transfer is favored on the CS, and, as a consequence, an improvement of the heat exchanger performance can be achieved by acting on the hot side.

The outlet temperatures of cold and hot fluids are illustrated in figures 17 and 18.

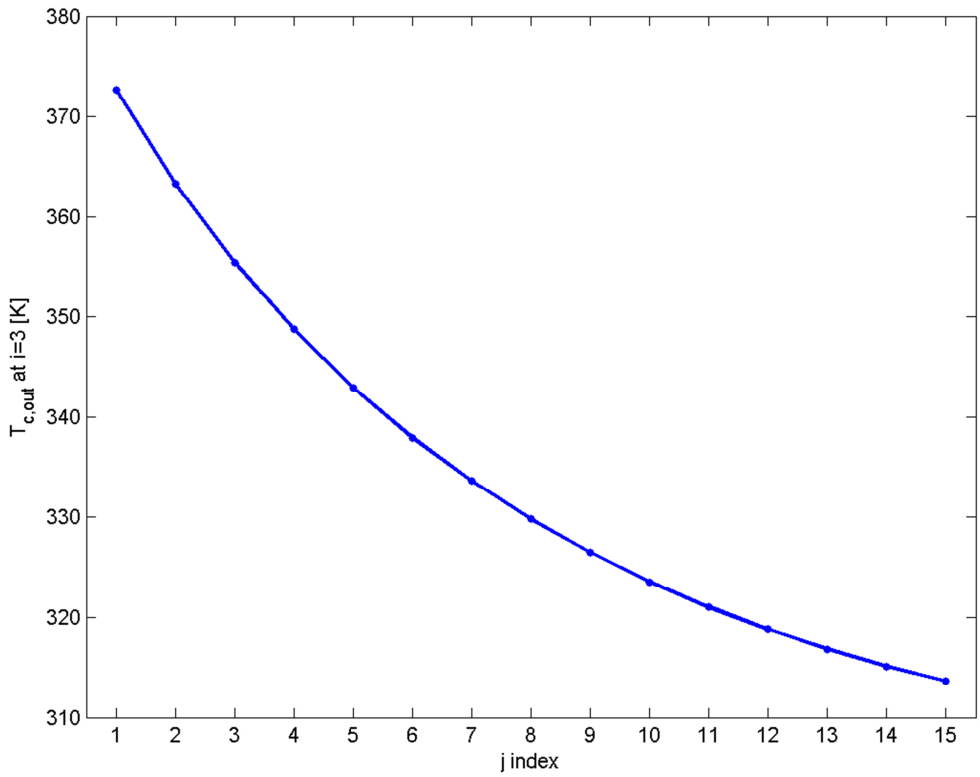

Figure 17. Cold fluid outlet temperature along the HS.

The temperature of cold fluid at the outlet (i=3) decreases along the hot fluid direction, getting the maximum value of 373 K at j=1 and the minimum of 314 K at j=15.

The hot fluid gets the minimum temperature, 322 K, at the inlet of cold fluid (i=1), while rises up to 337 K at the cold fluid exit (i=3).

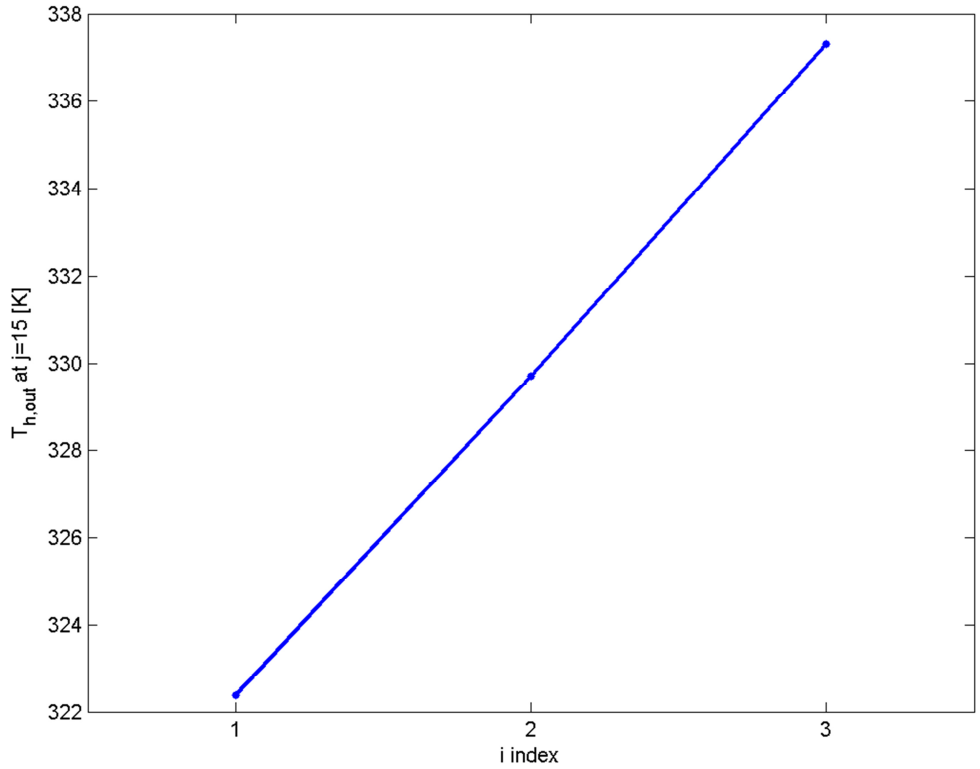

Figure 18. Hot fluid outlet temperature along the CS for the case study.

The corresponding mass averaged temperatures of cold and hot fluid at the outlet are obtained as:

$$T_{c,out} = \frac{\sum_{j=1}^{n} \dot{m}_c(j) \cdot T_{c,out}(3,j)}{\sum_{j=1}^{n} \dot{m}_c(j)} \tag{15}$$

$$T_{h,out} = \frac{\sum_{i=1}^{m} \dot{m}_h(i) \cdot T_{h,out}(i,15)}{\sum_{i=1}^{m} \dot{m}_h(i)} \tag{16}$$

The computed values of temperatures and the heat transfer rate of the layer are summarized in Tab.9.

Table 9. Outlet temperatures and heat transfer rate of the layer.

	Unit	
$T_{h,out}$	K	329.8
$T_{c,out}$	K	333.9
Q	W	819.6

The heat transfer rate computed with the hybrid method was compared with that obtained with the ε – *NTU* method applied to the same heat exchanger.

The convective heat transfer coefficient on both cold and hot sides was calculated via relationships found in literature [10] and [12]. The knowledge of the convective heat transfer coefficients on both sides allows to evaluate the overall heat transfer coefficient, and as consequence, the Number of Transfer Units, the effectiveness and the corresponding heat transfer rate (Tab.10).

Table 10. Results of ε – *NTU* method.

NTU	Effectiveness	Heat transfer rate [W]
8.14	0.65	676

The ε – *NTU* method led to an underestimation of the heat transfer rate with respect to the hybrid method, in this case of about 17%, and as a result, if adopted for design, to a corresponding oversizing of the heat exchanger.

The hybrid method is a multi-scale approach.

In order to evaluate the layer performance with a full scale approach, the mean wall temperature should be taken into account for computation.

The ε – *NTU* method is a full scale approach and the fluid properties are calculated at the film temperature, i.e. the mean of the inlet fluid and wall temperatures. If it was applied to the single UHTVs of the layer, taking into account the effective inlet fluid and wall temperatures, it would lead to a heat transfer rate value closer to that found with the hybrid method.

Actually, for the case study here presented, the mean wall temperature was found to be of 347.5 K. This value corresponds to that found at the cell (3,7), which is not the central one, as one might mistakenly think.

Another case, with the same heat transfer geometry and temperatures of the previous one, but with the mass flow rates in Tab.11, was analyzed. The mean wall temperature for Case B resulted in 330.3 K. The mean wall temperature is not a simple average between the cold and hot fluid temperatures at the inlet, but it is a result of the real distribution, and for this reason is different for each combination of operating conditions.

This demonstrates that the full scale approach involves a poorer level of accuracy.

Table 11. Mass flow rates for Case B.

	Unit	Hot fluid	Cold fluid
$\dot{m}$	kg/s	0.25	1.5

Conclusions

In this work, a method to investigate and find the overall performance of the heat exchanger starting from the CFD simulations at the micro-scale was proposed. A set of control volumes that include the finned surfaces of both the cold and hot sides (separated by a wall) were detected.

The results of the separate numerical modeling of the two finned surfaces carried out by Carluccio et al. [10] and [11] were used to get prediction functions through a purposely defined regression technique.

These functions allowed to predict the behavior of the sub-domain at different operating conditions, such as wall temperature, fluid inlet temperature and velocity.

The numerical modeling of the whole heat exchanger requires high computational cost, for this reason an iterative method has been adopted to evaluate with a high level of accuracy the performance of the whole system.

The new method called "hybrid" was described here in detail. Many considerations have been made that are clear when examining the results of its application to a case study:

- the heat transfer rate trend can be analyzed for each heat exchanger . For the case study, it was observed that the heat transfer rate is higher when approaching the cold fluid inlet for $j \leq 6$ while it improves near the cold fluid outlet for $j > 6$ (near the hot fluid exit). The heat transfer rate maximum and minimum values occur at positions (1,1) and (1,15).
- the investigations on the heat transfer coefficients allow to detect where the energy flux is higher, providing a valid support for the heat exchanger design. For the test case the convective coefficient is favored on the cold side and, as a consequence, the overall performance can be enhanced by acting on the hot side fin geometry.
- the multi-scale approach, adopted by the hybrid method, with respect to the full-scale one, applied by the $\varepsilon - NTU$ method, evaluates the overall performance taking into account the temperature and flow distributions. The heat transfer rate obtained by the hybrid method for the case study was compared with value calculated by the $\varepsilon - NTU$ method. This comparison shows that the full scale approach, leads to an underestimation of the heat transfer, and if used for design, to a conservative oversizing of the heat exchanger
- the hybrid method gives information about pressure losses through the heat exchanger either at hot or at cold side

The proposed innovative method can be used to investigate the overall performance of heat exchangers with different fins and working fluids at different operating conditions, by collecting either numerical or experimental data.

With obvious modifications, the same approach will be applied in future not only to cross flow heat exchangers, but also to other typologies (even more complex) of heat transfer devices.

References

[1] Kays, W.M., and. London, A.L. *Compact Heat Exchangers*. United States: McGraw-Hill, New York, NY, 1984. Print.

[2] Sekulić DP, Shah RK, Pignotti AA. A Review of Solution Methods for Determining Effectiveness-NTU Relationships for Heat Exchangers With Complex Flow Arrangements. ASME. Applied Mechanics Reviews, 1999, 52(3):97-117

[3] Navarro, H.A., and Luben, C.G.. "A new approach for thermal performance calculation of cross-flow heat exchangers." *International Journal of Heat and Mass Transfer* 48.18 (2005): 3880-3888.

[4] Sanders, Paul A., and Karen A. Thole. "Effects of winglets to augment tube wall heat transfer in louvered fin heat exchangers." *International Journal of Heat and Mass Transfer* 49.21 (2006): 4058-4069.

[5] Lawson, Michael J., and Karen A. Thole. "Heat transfer augmentation along the tube wall of a louvered fin heat exchanger using practical delta winglets." *International Journal of Heat and Mass Transfer* 51.9 (2008): 2346-2360.

[6] Bhutta, Muhammad M.A., Hayat, N., Bashir, M. H., Khan, A. R., Ahmad, K. N., and Khan, S. "CFD applications in various heat exchangers design: A review." A*pplied Thermal Engineering* 32 (2012): 1-12

[7] Ferouillat, S., Tochon, P., Garnier, C., and Peerhossaini, H. "Intensification of heat-transfer and mixing in multifunctional heat exchangers by artificially generated streamwise vorticity." *Applied Thermal Engineering* 26.16 (2006): 1820-1829.

[8] Stalio, E., and Piller, M. "Direct numerical simulation of heat transfer in converging–diverging wavy channels." *Journal of heat transfer* 129.7 (2007): 769-777.

[9] Ciuffini, A, Scattina, A, Carena, F, et al. Multiscale Computational Fluid Dynamics Methodology for Predicting Thermal Performance of Compact Heat Exchangers. ASME.*J. Heat Transfer.*2016; 138(7).

[10] Carluccio, E., Starace, G., Ficarella, A., and Laforgia, D. "Numerical analysis of a cross-flow compact heat exchanger for vehicle applications." *Applied Thermal Engineering* 25.13 (2005): 1995-2013.

[11] Starace, G., E. Carluccio, E., and Laforgia, D. "Automotive Compact Surpercharge-Air Intercooler Numerical Analysis." *International Heat Transfer Conference 13*. Begel House Inc., 2006.

[12] Manglik, R. M., and Bergles, A. E. "Heat transfer and pressure drop correlations for the rectangular offset strip fin compact heat exchanger." *Experimental Thermal and Fluid Science* 10.2 (1995): 171-180.